

Control of Proton and Electron Transfer in *de Novo* Designed, Biomimetic β Hairpins

Robin S. Sibert^{†,*}, Mira Josowicz[†], and Bridgette A. Barry^{†,*,*}

[†]Department of Chemistry and Biochemistry and ^{*}Petit Institute for Bioengineering and Bioscience, Georgia Institute of Technology, Atlanta, Georgia 30332

Beta hairpins are common secondary structural motifs found in proteins and have proven to be useful systems in which to quantify the noncovalent interactions involved in protein folding and protein interactions (reviewed in ref 1). Specifically, studies on model peptides have revealed that aromatic, cation- π , hydrophobic interactions and salt bridges play significant roles in stabilizing hairpin structure (1–8). Elucidation of structural elements, which facilitate β hairpin formation, has enabled *de novo* design of biomimetic peptides. These peptides can then serve as simple and functional models of more complex, native proteins (1, 9, 10).

Here, we employ *de novo* designed β hairpins to investigate how the protein environment controls proton coupled electron transfer (PCET) in enzymes. According to the nomenclature of refs 11 and 12, PCET refers to any chemical reaction in which an electron and a proton are transferred, regardless of mechanism. A similar model peptide approach has been used previously to explore the effect of noncovalent interactions on the redox potential of hemes, iron sulfur clusters, cofactors, and other metal centers in peptide models (13–17). Our previous work used a β hairpin peptide to study PCET reactions involving a redox-active tyrosine (Figure 1, panel A) (18).

Redox-active tyrosines are found in several enzymes, including photosystem II (PSII) (19, 20), ribonucleotide reductase (21), prostaglandin synthase (22), and galactose oxidase (23). In these proteins, a tyrosine side chain is transiently oxidized to form a neutral tyrosyl radical, Tyr[•] or Tyr^{ox}. Because the pK of the phenolic oxygen is dramatically altered by oxidation (24), redox-active tyrosines can participate in PCET reactions in proteins.

PSII contains two redox-active tyrosine residues, Tyr161D1 (TyrZ) and Tyr160D2 (TyrD) (19, 20). PSII

ABSTRACT Tyrosine side chains are involved in proton coupled electron transfer reactions (PCET) in many complex proteins, including photosystem II (PSII) and ribonucleotide reductase. For example, PSII contains two redox-active tyrosines, TyrD (Y160D2) and TyrZ (Y161D1), which have different protein environments, midpoint potentials, and roles in catalysis. TyrD has a midpoint potential lower than that of TyrZ, and its protein environment is distinguished by potential π -cation interactions with arginine residues. Designed biomimetic peptides provide a system that can be used to investigate how the protein matrix controls PCET reactions. As a model for the redox-active tyrosines in PSII, we are employing a designed, 18 amino acid β hairpin peptide in which PCET reactions occur between a tyrosine (Tyr5) and a cross-strand histidine (His14). In this peptide, the single tyrosine is hydrogen-bonded to an arginine residue, Arg16, and a second arginine, Arg12, has a π -cation interaction with Tyr5. In this report, the effect of these hydrogen bonding and electrostatic interactions on the PCET reactions is investigated. Electrochemical titrations show that histidine substitutions change the nature of PCET reactions, and optical titrations show that Arg16 substitution changes the pK of Tyr5. Removal of Arg16 or Arg12 increases the midpoint potential for tyrosine oxidation. The effects of Arg12 substitution are consistent with the midpoint potential difference, which is observed for the PSII redox-active tyrosine residues. Our results demonstrate that a π -cation interaction, hydrogen bonding, and PCET reactions alter redox-active tyrosine function. These interactions can contribute equally to the control of midpoint potential and reaction rate.

*Corresponding author,
bridgette.barry@chemistry.gatech.edu.

Received for review May 19, 2010
and accepted September 7, 2010.

Published online October 4, 2010

10.1021/cb100138m

© 2010 American Chemical Society

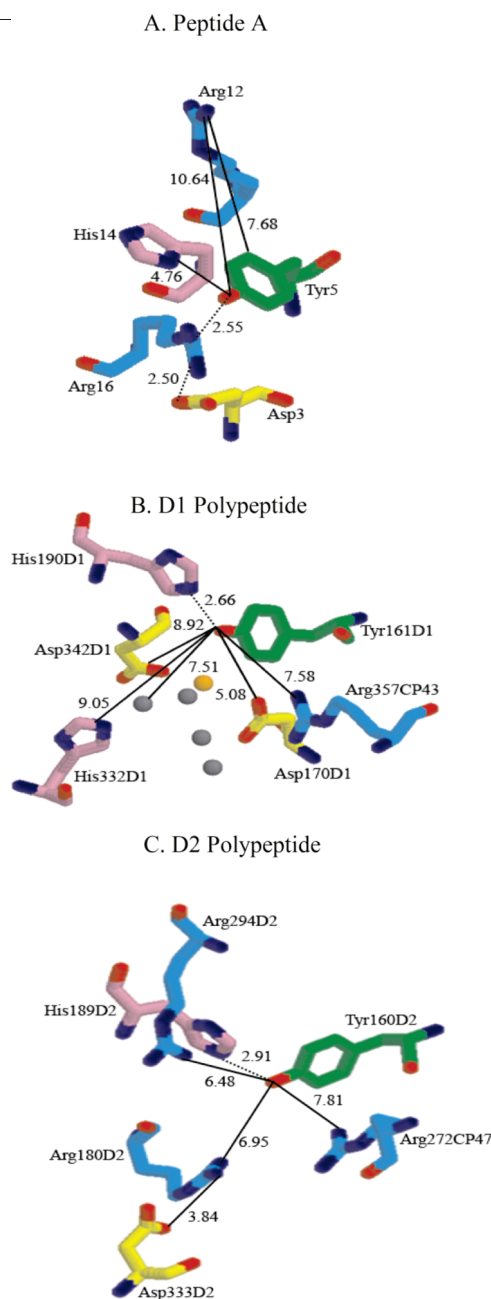


Figure 1. Environment of redox-active tyrosines in peptide A and in PSII. Panel A shows Tyr 5 in peptide A (18), panel B shows TyrZ in PSII, PDB ID 3BZ1 (37), and panel C shows TyrD in PSII, PDB ID 3BZ1 (37). The solid lines indicate distances between tyrosine and neighboring amino acids, and the dotted lines represent hydrogen bonds. The RasMol molecular visualization tool was used to depict histidine (violet), arginine (cyan), and aspartic acid (yellow) residues within 10.0 Å of the tyrosine (green). Manganese and calcium ions are shown in gray and orange, respectively, in panel B.

catalyzes the light-driven oxidation of water to form molecular oxygen. The two tyrosines are found in conserved positions in the PSII reaction center; these positions are linked by approximate C_2 symmetry. TyrZ is located in the D1 polypeptide of PSII (Figure 1, panel B). This redox-active tyrosine participates in water oxidation by reducing P_{680}^+ and oxidizing a tetranuclear calcium–manganese cluster (20, 25–28). TyrD (Figure 1, panel C) is located in the D2 polypeptide of PSII and is not required for oxygen evolution (19, 29). TyrD redox reactions may be involved in the assembly of the manganese cluster (19, 29, 30). TyrZ and TyrD have midpoint potentials that differ by ~ 200 mV (28, 31). The radicals have dramatically different decay times. TyrZ^{ox} has a microsecond to millisecond lifetime (32), whereas TyrD^{ox} has a lifetime on the order of minutes to hours (19). The protein environmental interactions, which give rise to these energetic and kinetic differences, are still not understood.

PCET reactions are associated with both TyrD and TyrZ, and the mechanism of these reactions may contribute to the observed, functional differences. Recent studies have shown that TyrD proton transfer reactions proceed with different mechanisms at high and low pH (33, 34). For TyrD, proton inventory and solvent isotope exchange have shown that a coupled PCET (CPET) mechanism occurs at high pH (34). In this type of reaction, the electron and proton are transferred simultaneously. Further, this previous work on TyrD has shown that reaction at high pH involve the transfer of multiple protons (33, 34). A study of PCET has also been reported for TyrZ in manganese-depleted PSII (35), which is inactive in water oxidation.

Crystal structures of cyanobacterial PSII (36, 37) show that the environments of TyrZ and TyrD differ in their distance from the calcium–manganese cluster. TyrZ is 4.8 Å from the calcium in the metal cluster (Figure 1, panel B), while TyrD is 28 Å away. The detailed placement of histidine, arginine, and aspartic acid side chains (Figure 1, panels B and C) also distinguishes the redox-active tyrosines. TyrZ is predicted to hydrogen bond with His190D1. TyrZ is 5.1 Å from Asp170D1, a possible manganese ligand, and 7.6 Å from Arg357CP43 (Figure 1, panel B). TyrZ may also interact electrostatically with a second histidine (His332D1) residue and a second aspartic acid (Asp342D1) residue (Figure 1, panel B), which potentially coordinate manganese (Figure 1, panel B). TyrD is predicted to form a

hydrogen bond with His189D2 and is 7.0 Å from a potential Asp333D2–Arg180D2 salt bridge. In addition, TyrD has potential π -cation interactions with Arg272 of the CP47 subunit, at 7.8 Å, and with Arg294 of the D2 subunit, at 6.5 Å (Figure 1, panel C). The corresponding arginines are not found in the environment of TyrZ (Figure 1, panel B). Possible effects of these π -cation interactions are the focus of this report.

The electron transfer rate in proteins is responsive to changes in distance and midpoint potential (38). A number of redox-active tyrosine model systems have been used to examine how function is controlled by the responsive protein matrix. Studies involving phenol derivatives with pendant bases have shown that hydrogen bonding alters the reduction potential of tyrosine (39). Tyrosine and tryptophan residues have been linked to ruthenium photosensitizers, which resulted in model complexes for proton-coupled electron transfer from amino acids (40, 41). Studies of tyrosine appended to ruthenium complexes have investigated the pH and buffer dependence of the PCET reactions (41). Electrochemistry has been used to examine PCET mechanism for the oxidation of phenols in water (42). In designed helical proteins, the redox potential of tyrosine was modulated by placement in a nonpolar environment and by shielding from proton acceptors (14, 43).

In a recent study, we described a β hairpin peptide, IMDRYRVRNGDRIHRLR (peptide A), in which PCET reactions between Tyr5 and His14 modified the midpoint potential of the single tyrosine residue (18). In peptide A, Tyr5 is hydrogen-bonded to an arginine residue, Arg16, and a second arginine, Arg12, has a π -cation interaction with the tyrosine (Figure 1, panel A). Oxidation of tyrosine causes a pK shift of His14, which will result in histidine protonation in the mid-pH range. This peptide exhibits an example of a PCET reaction in which the electron and proton acceptors are two distinct species. Although Tyr5 and His14 are not directly hydrogen-bonded, the PCET reaction between tyrosine and histidine can occur through a network of water molecules (18, 41, 42).

Here, we report results obtained from studies of four additional β hairpin peptides, in which substitutions were made at His14, Arg12, and Arg16. The results show that hydrogen bonding, π -cation, and PCET interactions alter the midpoint potential of redox-active tyrosines. In addition, hydrogen bonding and π -cation interactions with tyrosine alter the pH range over which PCET reac-

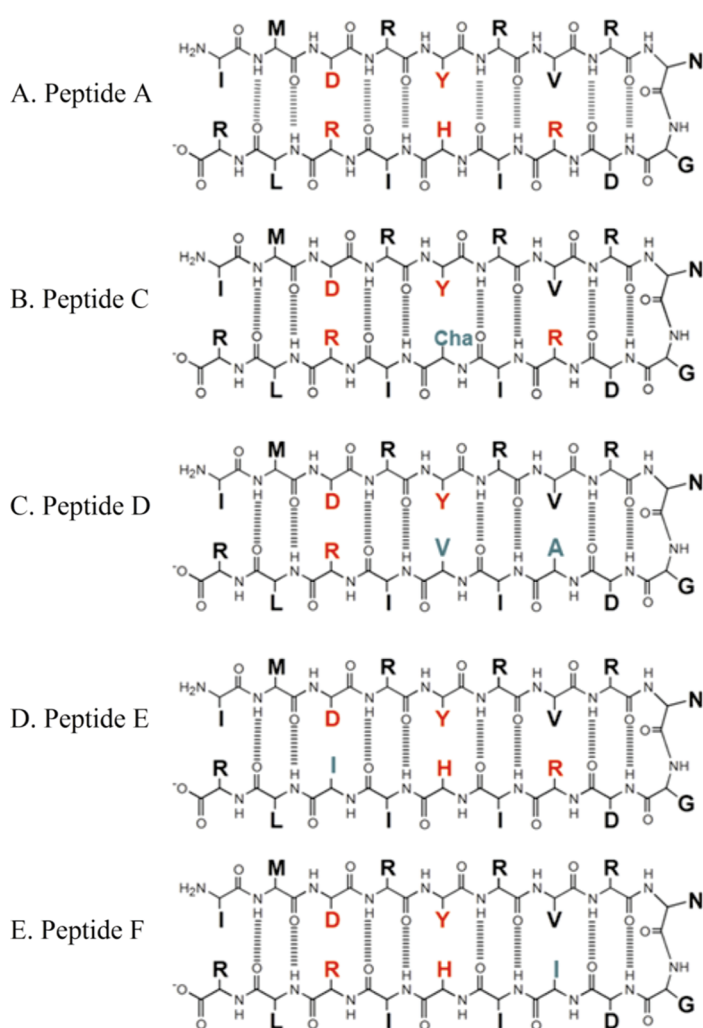


Figure 2. Predicted structures and cross strand interactions for β hairpin peptides. In peptide A, tyrosine and interacting residues are shown in red. Sequence alterations are shown in green in peptides C–F. The sequence of peptide B (IMDRYRVRNGDRIHRLR) is not shown because it was an unfolded control sequence.

tions occur. These results imply that differential placement of arginine residues can contribute to functional differences observed between TyrZ and TyrD.

RESULTS AND DISCUSSION

Peptide Design. Figure 2 shows the amino acid sequence and predicted cross-strand interactions for peptides A and C–F. The ProtParam tool was used to compute the physicochemical properties of the peptides (44). Sequences were predicted to be stable and soluble

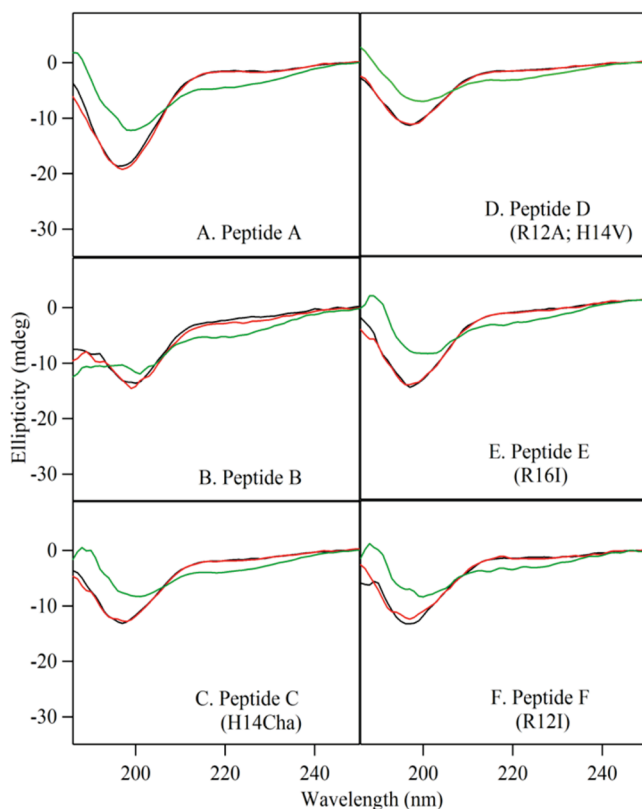


Figure 3. CD of β hairpin peptides at pH 5.0. The panels show data acquired from (A) peptide A, (B) peptide B, (C) peptide C (His14Cha), (D) peptide D (H14V; R12A), (E) peptide E (R16I), and (F) peptide F (R12I). The spectra were collected at 20 °C (red, premelt), 80 °C (green), and 20 °C (black, postmelt). See Methods for spectral conditions.

in water. The peptides were designed with a net charge of +1 or +2 at pH 11 ensure solubility and an isoelectric point (pI) of greater or equal to 11. Each peptide contains a single tyrosine residue, at least one salt bridge (3, 4), a type I' Asn-Gly turn (2, 45), and several amino acids with high propensities for forming β sheets (46). Peptide A, peptide E (Arg16Ile), and peptide F (Arg12Ile) also contain an aromatic interaction (2, 3, 45) between Tyr5 and His14.

In the NMR structure of peptide A (18), Tyr5 accepts a hydrogen bond from the ϵ -NH of Arg 16. The structure also showed a π -stacked aromatic interaction between Tyr5 and His14 and a possible π -cation interaction between Tyr5 and Arg12, which are 7.7 Å apart. In peptides C and D, His14 was replaced by cyclohexylalanine and valine, respectively (Figure 2). This replacement is ex-

pected to disrupt PCET reactions involving the histidine. In peptides E and F, Arg16 and Arg12 were substituted with Ile to assess the role of the hydrogen bond and π -cation interaction, respectively. Peptide D is a double mutant, in which His14 was replaced by valine, and Arg12 was substituted with Ala.

Circular Dichroism. Circular dichroism (CD) spectropolarimetry was used to verify that peptides C, D, E, and F form β hairpins in aqueous solution. Figure 3 presents the CD spectra of peptide A (panel A), peptide B (His14Val) (panel B), peptide C (His14Cha) (panel C), peptide D (His14Val; Arg12Ala) (panel D), peptide E (Arg16Ile) (panel E), and peptide F (Arg12Ile) (panel F). These experiments were conducted at pH 5.0, and thermal denaturation experiments were performed on each peptide. Peptide A (panel A) served as a folded control, because previous NMR experiments have shown that the peptide is folded at this pH (18). At 20 °C, the CD spectrum of peptide A (panel A, red) exhibited a minimum at 197 nm. At 80 °C, the amplitude decreased (panel A, green). Additionally, a second broad minimum appeared at 221 nm. The original CD spectrum was regained by cooling the sample back to 20 °C (panel A, black), and an isodichroic point was observed at 207 nm. On the other hand, the NMR spectra of peptide B (panel B) indicated that it is predominantly random coil; therefore, peptide B served as an unfolded control. As expected, at 20 °C, the CD spectrum of unfolded peptide B (panel B, red) displayed a shallow minimum at 200 nm, and only small changes were induced by heating (panel B, green).

At pH 5.0, peptide C (His14Cha) (panel C), peptide D (His14Val; Arg12Ala) (panel D), peptide E (Arg16Ile) (panel E), and peptide F (Arg12Ile) (panel F) all exhibited CD data and thermal denaturation, which were similar to peptide A. Thus, the data support the conclusion that peptides C–F form β hairpin structures at pH 5.0. CD spectra were also collected for the peptides at pH 11.0 (Supplementary Figure S1). These data support the conclusion that the peptides form β hairpin structures pH 11 (see Supporting Information for more details).

pK Determination. As discussed in the Supporting Information (Supplementary Figure S2), optical titration curves were used to measure the pK of tyrosine in peptides A, C, D, E, and F. As a control, the pK of tyrosine in solution was determined and found to be 9.8 ± 0.1 (Supplementary Figure S2A), which is similar to the value of 10.17 ± 0.02 reported in the literature (47).

The small variation may be due to differences in buffer conditions in the two experiments. The pK of Tyr5 in peptide A was measured to be 9.3 ± 0.1 (Supplementary Figure S2B). The pK values of tyrosine in peptides C, D, and F were similar to those of peptide A and were 9.6 ± 0.1 , 9.4 ± 0.3 , and 9.6 ± 0.1 , respectively (Supplementary Figure S2C, D, and F and Table 1). These data support the conclusion that His14 and Arg12 do not have a substantial influence on the dissociation constant of Tyr5. However, the titration curve for peptide E (Arg16Ile), in which the hydrogen bond to Arg16 is eliminated (Supplementary Figure S2E), contains two equivalence points. Fitting the low pH transition gave a pK of 8.3 ± 0.1 for the first equivalence point. These data show that the hydrogen bond to Arg16 alters the proton affinity of the phenolic oxygen. The presence of two pK values in peptide E (Arg16Ile) suggests that there are two possible sets of noncovalent interactions with Tyr5 in this peptide.

Electrochemical Titrations. To analyze the effects of noncovalent interactions on tyrosine oxidation, we performed electrochemical titrations of peptides C–F using square wave voltammetry (18). The potential for tyrosyl radical formation was plotted versus pH for each sample (Figure 4). As a control, fits were performed for tyrosine in solution, which should give a linear dependence of peak potential on pH below the phenolic pK (18). The tyrosine data could be fit with a derived slope of 67 ± 2 mV/pH unit and the pK of 9.8 derived from the optical data (Table 1). If the fits were conducted with the literature pK of 10.17 (47), the results were similar. The slope was 64 ± 1 mV/pH unit, the E^* value was 1.33 ± 0.01 , and the χ^2 value was 2.56×10^{-3} .

In the peptides, the side chains of aspartic acid, tyrosine, and histidine have pK values within the pH range of the electrochemical titration. pK shifts in these species can influence the pH dependence. The electrochemical data from the peptides (Figure 4 and Table 1) were fit with a Nernst equation in which one or more ionizable groups influence the potential (18), and χ^2 values were used to evaluate the quality of the least-squares fits (Table 1). Data in the Supporting Information illustrate this procedure for peptide F (Supplementary Figure S3 and Table S1), which is best fit with three ionizable groups. While the fits illustrated in Figure 4 adequately represent the data, the simulations cannot be regarded as unique fits.

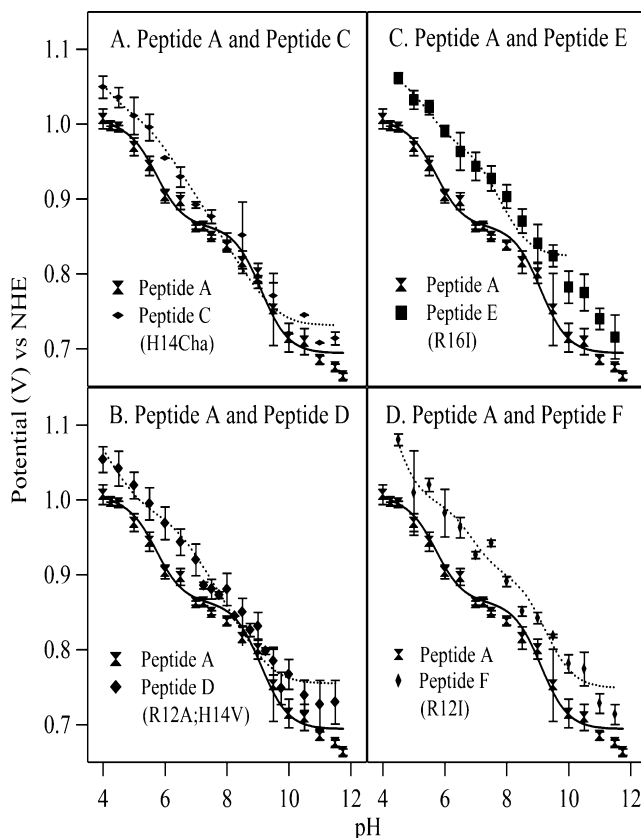


Figure 4. Electrochemical titrations of β hairpin peptides. The titration curve of peptide A is shown in each panel with a fit superimposed as a solid line (Table 1). The panels also show data acquired from (A) peptide C (H14Cha), (B) peptide D (H14V; R12A), (C) peptide E (R16I), and (D) peptide F (R12I), with fits superimposed as dotted lines. The error bars represent one standard deviation. See Table 1 for fit parameters and Methods for spectral conditions.

In fitting the electrochemical data from each peptide, the pK_{red} of Tyr was fixed at the pK derived for the corresponding sample by optical titration experiments (Supporting Information). The pK_{ox} of Tyr radical is -2 but was fixed at 0 for these calculations (18, 24). The data for peptide A were fit with the Nernst equation in which three ionizable groups (Asp3, Tyr5, and His14) influence the potential (Figure 4, solid lines). The fit to the peptide A data (Figure 4, solid lines) predicts inflection points at pH 2.8 (reduced state), 5.8 (oxidized state), 6.0 (reduced state), and pH 9.0 (oxidized state) (Table 1). Previously, we predicted similar pK values using a different fitting procedure (18). Using that method, the pK values were assigned as 0 (Tyr5), 4.5 (Asp3),

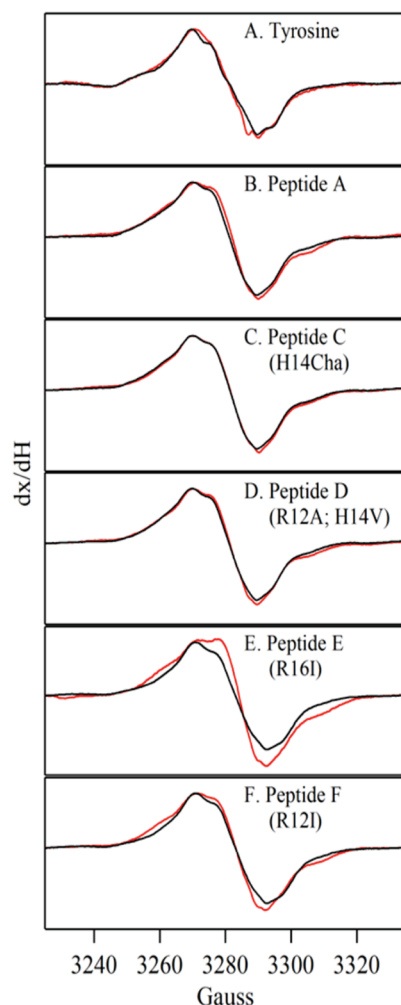


Figure 5. EPR spectra of tyrosyl radicals in β hairpin peptides at pH 5.0 (red) and 11.0 (black). The radicals were generated by UV photolysis at 108 K. The panels show spectra acquired from (A) tyrosine, (B) peptide A, (C) peptide C (H14Cha), (D) peptide D (H14Val; R12A), (E) peptide E (R16I), and (F) peptide F (R12I). To compare spectral line width, the spectra were normalized for any amplitude differences. See Methods for spectral conditions.

and 8.0 (His14) in the oxidized state and 10.0 (Tyr5), 4.0 (Asp3), and 7.0 (His14) in the reduced state (18).

In the present fit, the inflection points at pH 2.8 and 5.8 are attributed to Asp3 in the Tyr^{red} and Tyr^{ox} forms of the peptide, respectively (Table 1). This result is consistent with a tyrosine-oxidation induced electrostatic

perturbation of this amino acid. The inflection points at pH 6.0 and 9.0 are attributed to redox-induced changes in the proton affinity of His14 in the Tyr^{red} and Tyr^{ox} forms of the peptide, respectively (18). At pH values between 6 and 9, this result predicts that a histidine PCET reaction will occur, because His14 will protonate when Tyr5 is oxidized.

Figure 4 presents electrochemical data, acquired from peptide C (His14Cha) (panel A), peptide D (Arg12Ala; His14Val) (panel B), peptide E (Arg16Ile) (panel C), and peptide F (Arg12Ile) (panel D). Fits to the data are shown superimposed as the dotted line (Table 1). For comparison, electrochemical data derived from peptide A are also shown in each Figure 4 panel, with the fit superimposed as a solid line (Table 1).

As expected from the pK assignments, substitution at His 14 in peptide C (His14Cha) (Figure 4, panel A) eliminated the His 14 inflection points at pH 6.0 and 9.0 (Table 1), which were observed in peptide A. This result is consistent with our previous work (18), which showed that PCET reactions in peptide A involve His 14 as the proton acceptor. Removal of His14 in peptide C (His14Cha) increased the redox potential of Tyr5 at low pH values, as previously reported (18). The pK values of Asp3 were not significantly altered, given the standard deviations (Table 1).

Figure 4, panel C presents electrochemical titration data acquired from peptide E (Arg16Ile), in which the hydrogen bond between Arg16 and Tyr5 was eliminated. In peptide E (Arg16Ile) (panel C, dotted line), a significant ~ 50 mV change in midpoint potential was observed at all pH values, when the data were compared to peptide A (panel C, solid line). Fits to the data showed that the pK of His14 in the Tyr^{ox} form of peptide E (Arg16Ile) decreased from 9.0 to 7.9 (Table 1). However, removal of the Arg-Tyr hydrogen bond had no significant effect on the pK of His14 in the Tyr^{red} form of the peptide (Table 1). Table 1 also shows that the pK values for Asp 3 were not significantly altered.

Figure 4, panel D presents electrochemical titration data of peptide F (Arg12Ile) (dotted line), in which the putative π -cation interaction between Arg12 and Tyr5 was eliminated. The data exhibited inflection points similar to those observed in peptide A (solid line). In peptide F (Arg12Ile) (dotted line), a significant ~ 50 mV change in midpoint potential was observed at all pH values, when the data were compared to peptide A (solid line). Substitution at Arg12 increased the pK (1.3 pH

TABLE 1. Parameters used to fit the electrochemical titration data on peptides

Sample	E^* (V) ^a	S (V/pH) ^a	Tyr ^{ox}	Asp ^{ox a}	His ^{ox a}	Tyr ^{red}	Asp ^{red a}	His ^{red a}	χ^2 ^a
Tyrosine ^b	1.35 ± 0.01	0.067 ± 0.002	0.0			9.8 ± 0.1			2.91 × 10 ⁻³
Peptide A ^c	2.5 ± 0.2	0.6 ± 0.1	0.0	5.8 ± 0.6	9.0 ± 0.1	9.3 ± 0.1	2.8 ± 0.9	6.0 ± 0.6	1.78 × 10 ⁻³
Peptide C ^d (H14Cha)	1.33 ± 0.04	0.07 ± 0.01	0.0	5.6 ± 1.2		9.6 ± 0.1	4.6 ± 1.0		5.68 × 10 ⁻³
Peptide D ^d (R12A; H14 V)	1.6 ± 0.3	0.12 ± 0.07	0.0	7.3 ± 0.8		9.4 ± 0.3	5.2 ± 0.5		5.95 × 10 ⁻³
Peptide E ^c (R16I)	2.5 ± 0.3	0.4 ± 0.1	0.0	5.6 ± 0.2	7.9 ± 0.1	8.3 ± 0.1	3.4 ± 0.2	5.9 ± 0.2	2.22 × 10 ⁻³
Peptide F ^c (R12I)	2.1 ± 0.1	0.24 ± 0.01	0.0	6.8 ± 0.6	9.0 ± 0.1	9.6 ± 0.1	4.5 ± 0.3	7.3 ± 0.5	6.36 × 10 ⁻³

^aParameters were derived by performing a least-squares fit using Igor Pro software. The χ^2 values were used to evaluate the fits. The pK values reported for Tyr^{red} and Tyr^{ox} were determined from the optical titration data (Tyr^{red}) (Supplementary Figure S2) and from the literature (Tyr^{ox}) (24). ^bThe data were fit to the Nernst equation: $E_m = E^* - S \log\left[\frac{[10^{-pK_{ox}} + 10^{-pH}]}{[10^{-pK_{red}} + 10^{-pH}]}\right]$, which describes the influence of one ionizable group on the midpoint potential of tyrosine (18, 58). ^cThe data were fit to the modified Nernst equation: $E_m = E^* - S \log\left[\frac{([10^{-pH}]^3 + ([10^{-pH}]^2 \cdot [10^{-pK_{ox1}}]) + ([10^{-pH}] \cdot [10^{-pK_{ox1}}] \cdot [10^{-pK_{ox2}}]) + ([10^{-pK_{ox1}}] \cdot [10^{-pK_{ox2}}] \cdot [10^{-pK_{ox3}}]))}{([10^{-pH}]^3 + ([10^{-pH}]^2 \cdot [10^{-pK_{red1}}]) + ([10^{-pH}] \cdot [10^{-pK_{red1}}] \cdot [10^{-pK_{red2}}]) + ([10^{-pK_{red1}}] \cdot [10^{-pK_{red2}}] \cdot [10^{-pK_{red3}}]))}\right]$ which describes the influence of three ionizable groups on the midpoint potential of tyrosine (18, 58). ^dThe data were fit to the modified Nernst equation: $E_m = E^* - S \log\left[\frac{([10^{-pH}]^2 + ([10^{-pH}] \cdot [10^{-pK_{ox1}}]) + ([10^{-pK_{ox1}}] \cdot [10^{-pK_{ox2}}]))}{([10^{-pH}]^2 + ([10^{-pH}] \cdot [10^{-pK_{red1}}]) + ([10^{-pK_{red1}}] \cdot [10^{-pK_{red2}}]))}\right]$, which describes the influence of two ionizable groups on the midpoint potential of tyrosine (18, 58).

unit) of His 14 in the Tyr^{red} form of the peptide (Table 1) but caused no significant change in the pK of His14 in the oxidized form of the peptide. The pK of Asp3 increased in the Tyr^{red} (1.7 pH unit) forms of peptide F but not significantly in the Tyr^{ox} form (Table 1).

Figure 4, panel B presents electrochemical titration data of peptide D (Arg12Ala; His14Val) (dotted line), which contains a double substitution at His14 and Arg12. Inflection points due to His14 were not observed, as expected from comparison to the single His variant, peptide C (His14Cha) (panel A, dotted line). In addition, a ~50 mV increase in potential was observed at low pH, and a possibly significant increase in potential was also observed at high pH. This result is expected from comparison to results obtained on peptide C (His14Cha) (panel A, dotted line) and peptide F (R12I) (panel D, dotted line). In peptide D, the pK of Asp increased 1.5 pH units in the Tyr^{ox} form of the peptide and 2.4 pH units in the Tyr^{red} form of the peptide (Table 1).

Electron Paramagnetic Resonance (EPR)

Spectroscopy. A tyrosyl radical can be generated in tyrosine solutions and in the β hairpin peptides by UV photolysis (48, 49). The resulting neutral radical has electron spin density on the 1', 3', and 5' carbon atoms of the aromatic ring and on the phenolic oxygen (19, 50). Changes in the electron spin density distribution and in the conformation at the C _{β} -C1' dihedral angle can be detected as changes in EPR line shape (19, 50).

Figure 5, panel A presents the EPR spectrum of the tyrosyl radical in tyrosine solution at pH 5.0 (panel A, red) and 11.0 (panel A, black), respectively. As expected, tyrosine solutions exhibited an EPR spectrum with a g value of 2.0042, an overall splitting of ~20 G, and partially resolved hyperfine splittings (50). EPR spectra obtained from peptide A, C, D, and F were indistinguishable at pH 5.0 (Supplementary Figure S4B, C, and E). This result suggests that the immediate structure around the tyrosyl radical is similar in all four peptides. Peptide E showed a small change in EPR line shape at pH 5.0, when compared to the signal observed in peptide A (Supplementary Figure S4D). Small changes in EPR line shape, when peptide A and E are compared, are most likely due to slightly different tyrosyl radical conformations in the two peptides (18, 50). In tyrosine solutions (panel A) and peptide A (panel B), peptide C (panel C), peptide D (panel D), and peptide F (panel F), the EPR spectrum of the tyrosyl radical exhibited no significant pH-induced changes. However, in peptide E, in which the hydrogen bond between Arg16 and Tyr5 was eliminated, a pH-induced change in EPR line shape was observed (panel E), again most likely due to a different conformation at the C _{β} -C1' bond. In agreement with the results of optical titration on this peptide (Supplementary Figure S2), this result suggests two alternate sets of noncovalent interactions with Tyr 5 in this peptide.

Summary of Structural Characterization of β Hairpin Peptides.

We designed four 18-amino-acid polypeptides, in which we investigated the effect of noncovalent interactions on tyrosine redox properties. CD was used to verify that the peptides form β hairpins in aqueous solution. The NMR structure of peptide A confirmed that this peptide adopts a twisted β hairpin conformation at pH 5.0 (18), and its CD spectrum exhibited a well-defined minimum at 197 nm. The CD data of peptides C–F also exhibited minima at 197 nm, demonstrating that these peptides fold to form twisted β hairpins. While β sheets in proteins commonly exhibit a CD minimum at 210 nm, atypical CD spectra have been described for monomeric β hairpins previously (51–53).

Thermal denaturation experiments supported the conclusion that peptides C–F fold to form β hairpins in solution. As expected, peptide A exhibited reversible thermal denaturation between 20 and 80 °C at pH 5.0. This result is unlikely to occur in an unordered or random coil peptide. Moreover, the 20 and 80 °C CD spectra of peptides A, C (His14Cha), D (Arg12Ala; His14Val), E (Arg16Ile), and F (Arg12Ile) exhibited an isodichroic point at 207 nm. An isodichroic point is indicative of a two-state folding transition (54).

Taken together, the CD data supported the conclusion that peptides A, C (His14Cha), D (Arg12Ala; His14Val), and E (Arg16Ile) formed stable β hairpin structures at pH 5.0 and at pH 11.0. Peptide F (Arg16Ile) also formed a stable β hairpin at pH 5.0. At pH 11.0, peptide F formed a stable hairpin after heating and cooling, indicating that this peptide folds at pH 11 under some conditions (see Supporting Information).

The EPR spectra of tyrosyl radicals in the peptides provided information concerning the structure of Tyr5 in the oxidized form of the peptide. These data indicated that the immediate environment and conformation of the tyrosyl radical are similar in most of the peptides. Therefore, the functional differences observed are not likely due to unintended structural changes, other than the mutation. In peptide E, a small pH induced change in EPR line shape was observed. The change in the tyrosyl radical spectrum was consistent with a small pH-induced alteration in single bond $C_{\beta}-C_{1'}$ conformation in the peptide E tyrosyl radical.

Substitutions at Arg16 Increase Tyrosine Midpoint Potential and Alter PCET Mechanism. The NMR structure of peptide A showed that Arg16 and Tyr5 form a hydrogen bond in which Tyr5 is hydrogen-bonded as the

proton acceptor (18). Elimination of the hydrogen bond between Arg16 and Tyr5 caused a 50 mV increase in potential at all examined pH values. The observed increase in potential can be rationalized because oxidation of tyrosine has been shown to result in the migration of electron density to the phenolic oxygen of the radical (18). The effect on midpoint potential in peptide E (Arg16Ile) is consistent with stabilization of electron density on the tyrosyl radical phenolic oxygen through the Arg16–Tyr5 hydrogen bond in peptide A (18).

Substitution at Arg16 altered the pK of His14 in the oxidized state of peptide E (Arg16Ile) but not in the reduced form. The decrease in His pK is consistent with removal of a hydrogen bond between Arg16 and the tyrosyl radical at Tyr 5. In the absence of positively charged Arg16, there will be a decrease in negative charge on the Tyr5 phenolic oxygen. This may, in turn, decrease the stability of positive charge on the cross-strand imidazole side chain. This result implies that the hydrogen bond to Arg16 is preserved when the tyrosyl radical is formed in peptide A. However, the differential effect on the His14 pK suggests that the strength of the Tyr5–Arg16 hydrogen bond is altered by tyrosine oxidation.

Substitutions at Arg12 Increase Tyrosine Midpoint Potential and Alter PCET Mechanism. The NMR structure of peptide A suggested that Arg12 and Tyr5 have a π -cation interaction (18). In our electrochemical titrations, elimination of the putative electrostatic interaction between Arg12 and Tyr5 (peptide F, (Arg12Ile)) gave a 50 mV increase in potential at all examined pH values. The observed increase in potential can be rationalized as destabilization of electron density on the tyrosyl radical phenolic oxygen by removal of the interaction with the positive charge. These data suggest that π -cation interactions with redox-active tyrosines can significantly alter tyrosine midpoint potential in enzymes.

Peptide F (Arg12Ile) exhibited a significant increase in Asp pK in the Tyr^{red} peptide. Peptide D (Arg12Ala; His14Val), which contains substitutions at both His14 and Arg12, showed increases in Asp3 pK in both the Tyr^{ox} and Tyr^{red} form of the peptide. These alterations in Asp3 pK values may be due to small changes in the Arg16/Asp3 salt bridge distance in these peptides, relative to peptide A.

In peptide F (Arg12Ile), the derived pK of histidine in the Tyr^{red} form increased, but there was no significant ef-

fect on the His pK in the Tyr^{ox} form. The effect on the His14 pK in the Tyr^{red} form is consistent with removal of the histidine's interaction with the positive charge on Arg12, which will favor the protonated histidine side chain over a broader pH range. The differential effect in the oxidized and reduced forms of the peptide suggests that there is a change in His14–Arg12 distance in the oxidized form of the peptide, with a resulting decrease in the impact of the π -cation interaction on the tyrosyl radical. This result demonstrates that a π -cation interaction with tyrosine can alter the mechanism of PCET reactions in enzymes.

Comparison with PSII Tyrosyl Radicals. PSII contains two redox-active tyrosines, TyrZ (Figure 1, panel B) and TyrD (Figure 1, panel C). The midpoint potential of TyrZ (28) is ~ 200 mV higher than the potential of TyrD (31). Both tyrosines are predicted to hydrogen bond to histidine (37). Therefore, the detailed placement of other amino acids and metal ions in the protein environment must account for the observed potential difference. Figure 1, panels B and C show that the placement of arginine residues may contribute to functional differences between the two redox-active tyrosines. For TyrZ (panel B), Arg357 in the CP43 subunit is 7.6 Å away. For TyrD (panel C), Arg180 in the D2 polypeptide is 7.0 Å away, a second arginine, Arg272 in the CP47 subunit, is located 7.8 Å away, and a third arginine, Arg294 in the D2 polypeptide is located at 6.5 Å. Near TyrZ, Arg357 has a possible interaction with Asp170D1, a metal ligand, and, near TyrD, Arg180 has a salt bridge interaction with Asp333 in the D2 polypeptide.

Therefore, the PSII structure (37) suggests that Arg294 in the D2 polypeptide and Arg272 in the CP47 subunit may have π -cation interactions with the TyrD tyrosyl radical (panel C). While the distance between TyrD and Arg272 is 7.8 Å, in other proteins, π -cation interactions occur over distances as long as 10 Å with most π -cation pairs separated by 6 Å or less (55). From previous studies, a π -cation interaction would be expected to contribute ~ 13 mV (6) to the decrease in potential observed when TyrD and TyrZ are compared. However, our results show a larger contribution of ~ 50 mV is also possible. Therefore, π -cation interactions could make a substantial contribution to the midpoint potential difference observed for the PSII tyrosyl radicals.

Substitutions at His14 Change the Mechanism of the PCET Reactions. Peptides in which substitutions were made at His14 eliminated inflection points, attributed to imidazole protonation, in the electrochemical titration data. On the other hand, alterations at Arg12 and Arg16 did not eliminate the inflection points. This observation is consistent with our previous conclusion that oxidation of Tyr5 in peptide A is thermodynamically coupled with PCET to the histidine (18). Because the pK of His14 increased with tyrosine oxidation, protonation of histidine will occur between pH 6 and 9 when the tyrosine is oxidized. This oxidation-induced protonation of His 14 is an example of a PCET reaction, in which the electron goes to one acceptor (solvent) and the proton goes to a second acceptor, the imidazole ring.

Our electrochemical data showed that the effect of histidine protonation was to decrease the potential of the tyrosine at low pH values. This has been previously attributed to electrostatic stabilization of electron density on the phenolic oxygen (18) in the tyrosyl radical. Because Tyr5 and His14 are not hydrogen-bonded, the PCET reaction likely occurs through a network of water molecules between Tyr5 and His14. Previous nanosecond transient absorption spectroscopy on tyrosine-containing ruthenium and rhenium complexes has shown that proton transfer can occur to solvent water (41). Previous electrochemical studies have focused on the PCET reactions for phenol and have also shown that water can act as a proton acceptor (42).

The mechanism of PCET in peptide A has not as yet been elucidated. Formation of a tyrosyl cation radical, by sequential electron and proton transfer reactions, is predicted to be unfavorable (39–42). Therefore, PCET to histidine in peptide A may involve coupled, simultaneous motion of a proton and electron (CPET). A CPET mechanism has been inferred for tyrosine/phenol model compounds under some conditions (39–42), for TyrZ at low pH (35), and for TyrD at high pH (34). Future experiments will address this point.

Conclusions. Our studies of β hairpin peptides provide a model for PCET reactions in proteins. In β hairpin peptide A, proton transfer occurs to a cross strand histidine when tyrosine is oxidized. The tyrosine and histidine are not directly hydrogen-bonded, but PCET can occur through bridging solvent. A hydrogen bond to tyrosine or a π -cation interaction with tyrosine causes decreases in midpoint potential. Hydrogen bonding and

π -cation interactions also alter the mechanism of the PCET reactions. Protonation of the histidine, the π -cation

interaction, and the hydrogen bond contribute equally to the alteration in midpoint potential.

METHODS

Peptide Synthesis. Peptide A (IMDRYVRNGDRIHRLR), peptide B (IMDRYVRNGDRIVRLR), peptide C (His14Cha) (IMDRYVRNGDRI[Cha]RLR), peptide D (His14Val; Arg12Ala) (IMDRYVRNGDAIVRLR), peptide E (Arg16Ile) (IMDRYVRNGDRIHILR), and peptide F (Arg12Ile) (IMDRYVRNGDIIHRLR) were synthesized by Sigma Genosys. The peptides were purified to 95% homogeneity by the manufacturer. Mass spectrometry was used to verify the sequence, and the purity was determined by analysis of the reverse phase HPLC chromatogram.

Circular Dichroism (CD). A JASCO J-810 CD spectropolarimeter equipped with a thermostatted cell holder was employed. CD samples were prepared to concentrations between 0.1 and 0.2 mM in 5 mM acetate buffer at pH 5.0 or 5 mM borate buffer at pH 11.0. Solutions were filtered using Acrodisc 25 mm syringe filters with a 0.45 μ m HT Tuffryn membrane prior to data collection. The spectra were collected between 186 and 250 nm in 1 mm quartz cells at a scan speed of 50 nm/min (56, 57). Four to twelve scans were averaged to generate each spectrum, and three to five spectra on different samples were collected and averaged. A baseline was recorded using 5 mM acetate-NaOH, pH 5.0 buffer or 5 mM borate-NaOH, pH 11 buffer, and the baseline was subtracted manually. Spectral conditions were as follows: sensitivity, 100 mdeg; data pitch, 1 nm; scanning mode, continuous; scan speed, 50 nm/min; response time, 1 s; bandwidth, 1 nm.

Electrochemistry. Square wave voltammetry measurements were performed on a computer-controlled CH instruments, Inc. workstation (18). The experiments were conducted in a three-electrode cell, equipped with a 3 mm glassy carbon working electrode from Bioanalytical Systems, Inc., a platinum counter electrode, and a reference electrode (Ag/AgCl in 1 M KCl, $E = 0.22$ V (NHE)). The peptide sample concentrations were 0.05 mM in 0.2 M KCl and 10 mM sodium acetate-NaOH (pH 4.5–5.5), 10 mM sodium phosphate-NaOH (pH 6.0–7.5), 10 mM boric acid-NaOH (pH 8.0–9.5) or 10 mM CAPS-NaOH (pH 10.0–11.5). For tyrosine samples, acetate, phosphate, borate and CAPS were also used as the buffer. The sample was purged with nitrogen gas before data collection for 5 min. The data was collected in the presence of N_2 gas. The number of trials was two for tyrosine, two for peptides A and C, six for peptide D, and three for peptides E and F.

Oxidation was initiated with a holding time of 2 s at 0.1 V and then scanned up to 1.1 V. Data were collected in increments of $\Delta E = 0.004$ V. The square wave frequency, f , was 5 Hz, and the amplitude, A , of the applied pulse was 0.025 V (scan rate $v = fA = 125$ mV/s). The data were fit to a baseline manually, and the centroid was used to derive the peak potential.

Electron Paramagnetic Resonance (EPR) Spectroscopy. EPR spectra were collected on a Bruker EMX spectrometer equipped with a standard TE cavity. Spectra were recorded at 108 K using a Wilmad flow-through liquid nitrogen Dewar (48, 49). The samples were prepared to a concentration of 1 mM at pH 5.0 and pH 11.0 in 5 mM sodium phosphate-NaOH, pH 5.0 buffer or 5 mM boric acid-NaOH, pH 11.0 buffer. The tyrosyl radical was generated by 266 nm photolysis (48, 49). Baseline correction of the spectra was performed using Igor Pro software. The samples were flashed in the EPR cavity with fifty laser flashes with a pulse energy of 50–60 mJ. Spectral conditions were as follows: microwave frequency, 9.2 GHz; microwave power,

200 μ W; modulation amplitude, 3 G; modulation frequency, 100 kHz; scan time, 168 s; number of scans, 4; time constant, 655 ms. Data were obtained for two different samples and were averaged. At pH 5.0, the g values for the radicals were indistinguishable: 2.0042 for tyrosine solution, 2.0037 for peptide A, 2.0041 for peptide C (His14Cha), 2.0043 for peptide D (Arg12Ala; His14Val), 2.0037 for peptide E (Arg16Ile), and 2.0043 for peptide F (Arg12Ile). At pH 11.0, the g values for the radicals were also indistinguishable: 2.0042 for tyrosine solution, 2.0042 for peptide A, 2.0041 for peptide C (His14Cha), 2.0043 for peptide D (Arg12Ala; His14Val), 2.0043 for peptide E (Arg16Ile), and 2.0044 for peptide F (Arg12Ile).

Acknowledgment: The authors thank N. Hud and the members of his lab for use of the circular dichroism spectropolarimeter. This project was supported by Award Number R01GM043273 from the National Institute of General Medical Sciences and the National Eye Institute. The content is solely the responsibility of the authors.

Supporting Information Available: This material is available free of charge via the Internet at <http://pubs.acs.org>.

REFERENCES

- Robinson, J. (2008) Beta-hairpin peptidomimetics: Design, structures, and biological activities, *Acc. Chem. Res.* 41, 1278–1288.
- Tatko, C. D., and Waters, M. L. (2002) Selective aromatic interactions in β -hairpin peptides, *J. Am. Chem. Soc.* 124, 9372–9373.
- Kiehna, S. E., and Waters, M. L. (2003) Sequence dependence of β -hairpin structure: Comparison of a salt bridge and an aromatic interaction, *Protein Sci.* 12, 2657–2667.
- Ciani, B., Jourdan, M., and Searle, M. S. (2003) Stabilization of β -hairpin peptides by salt bridges: Role of preorganization in the energetic contribution of weak interactions, *J. Am. Chem. Soc.* 125, 9038–9047.
- Tatko, C. D., and Waters, M. L. (2004) Comparison of C-H \cdots π and hydrophobic interactions in a β -hairpin: Impact on stability and specificity, *J. Am. Chem. Soc.* 126, 2028–2034.
- Tatko, C. D., and Waters, M. L. (2004) The geometry and efficacy of cation- π interactions in a diagonal position of a designed β hairpin, *Protein Sci.* 12, 2443–2452.
- Skwierawska, A., Makowska, J., Oldziej, S., Liwo, A., and Scheraga, H. (2009) Mechanism of formation of the C-terminal β -hairpin of the B-3 domain of the immunoglobulin binding protein G from *Streptococcus*. I. Importance of hydrophobic interactions in stabilization of β hairpin structure, *Proteins: Struct., Func., Bioinf.* 75, 931–953.
- Riemen, A., and Waters, M. (2009) Design of highly stabilized β -hairpin peptides through cation- π interactions of lysine and N-methyllysine with an aromatic pocket, *Biochemistry* 48, 1525–1531.
- Hughes, R., and Waters, M. (2006) Model systems for β -hairpins and β -sheets, *Curr. Opin. Struct. Biol.* 16, 514–524.
- Rotondi, K., and Gierasch, L. (2006) Natural polypeptide scaffolds: β -sheets, β -turns, and β -hairpins, *Biopolymers* 84, 13–22.
- Huynh, M. H. V., and Meyer, T. J. (2007) Proton-coupled electron transfer, *Chem. Rev.* 107, 5004–5064.
- Costentin, C. (2008) Electrochemical approach to the mechanistic study of proton-coupled electron transfer, *Chem. Rev.* 108, 2145–2179.

13. Gibney, B., Rabanal, F., Skalicky, J., Wand, J., and Dutton, P. (1997) Design of a unique protein scaffold for maquettes, *J. Am. Chem. Soc.* **119**, 2323–2324.
14. Tommos, C. S., Skalicky, J. J., Pilloud, D. L., Wand, J., and Dutton, L. (1999) De novo proteins as models of radical enzymes, *Biochemistry* **38**, 9495–9507.
15. Discher, B. M., Noy, D., Strzalka, J., Ye, S., Moser, C. C., Lear, J. D., Blasie, J. K., and Dutton, L. P. (2005) Design of amphiphilic protein maquettes: Controlling assembly, membrane insertion, and cofactor interactions, *Biochemistry* **44**, 12344–12354.
16. Koder, R. L., and Dutton, P. L. (2006) Intelligent design: The de novo engineering of proteins with specified functions, *Dalton Trans.* 3045–3051.
17. Antonkine, M. L., Koay, M. S., Epel, B., Breitenstein, C., Gupta, O., Gärtner, W., Bill, E., and Lubitz, W. (2009) Synthesis and characterization of de novo designed peptides modelling the binding sites of [4Fe-4S] clusters in photosystem I, *Biochim. Biophys. Acta* **1787**, 995–1008.
18. Sibert, R., Josowicz, M., Porcelli, F., Veglia, G., Range, K., and Barry, B. A. (2007) Proton-coupled electron transfer in a biomimetic peptide as a model of enzyme regulatory mechanisms, *J. Am. Chem. Soc.* **129**, 4393–4400.
19. Barry, B., and Babcock, G. T. (1987) Tyrosine radicals are involved in the photosynthetic oxygen evolving system, *Proc. Nat. Acad. Sci. U.S.A.* **84**, 7099–7103.
20. Boemer, R. J., and Barry, B. A. (1993) Isotopic labelling and EPR spectroscopy show that a tyrosine residue is the terminal electron donor, Z, in manganese-depleted photosystem II preparations, *J. Biol. Chem.* **268**, 17151–17154.
21. Sjöberg, B.-M., Reichard, P., Graslund, A., and Ehrenberg, A. (1978) The tyrosine free radical in ribonucleotide reductase from *Escherichia coli*, *J. Biol. Chem.* **253**, 6863–6865.
22. Kulmacz, R. J., Ren, Y., Tsai, A.-L., and Palmer, G. (1990) Prostaglandin H synthase: Spectroscopic studies of the interaction with hydroperoxides and with indomethacin, *Biochemistry* **29**, 8760–8771.
23. Whittaker, M., and Whittaker, J. (1990) A tyrosine-deprived free radical in apogalactose oxidase, *J. Biol. Chem.* **265**, 9610–9613.
24. Dixon, W., and Murphy, D. (1976) Determination of the acidity constants of some phenol radical cations by means of electron spin resonance, *J. Chem. Soc., Perkins Trans.* **72**, 1221–1229.
25. Babcock, G. T., Blankenship, R. E., and Sauer, K. (1976) Reaction kinetics for positive charge accumulation on the water side of chloroplast photosystem II, *FEBS Lett.* **61**, 286–289.
26. Debus, R., Bary, B., Sithole, I., Babcock, G., and McIntosh, L. (1988) Directed mutagenesis indicates that the donor to P₆₈₀⁺ in photosystem II is tyrosine-161 of the D1 polypeptide, *Biochemistry* **27**, 9072–9074.
27. Gerken, S., Brettel, K., Schlodder, E., and Witt, H. T. (1988) Optical characterization of the immediate donor to Chlorophyll a₁₁⁺ in O₂-evolving photosystem II complexes, *FEBS Lett.* **237**, 69–75.
28. Metz, J. G., Nixon, P. J., Rögner, M., Brudvig, G. W., and Diner, B. A. (1989) Directed alteration of the D1 polypeptide of photosystem II: evidence that tyrosine-161 is the redox component, Z, connecting the oxygen-evolving complex to the primary electron donor, P680, *Biochemistry* **28**, 6960–6969.
29. Debus, R. J., Barry, B. A., Babcock, G. T., and McIntosh, L. (1988) Site-specific mutagenesis identifies a tyrosine radical involved in the photosynthetic oxygen-evolving complex, *Proc. Nat. Acad. Sci. U.S.A.* **85**, 427–430.
30. Ananyev, G., Sakiyan, I., Diner, B. A., and Dismukes, G. (2002) A functional role for tyrosine-D in assembly of the inorganic core of the water oxidase complex of photosystem II and the kinetics of water oxidation, *Biochemistry* **41**, 974–980.
31. Boussac, A., and Etienne, A. L. (1984) Midpoint potential of Signal II (Slow) in Tris-washed photosystem-II particles, *Biochim. Biophys. Acta* **766**, 576–581.
32. Dekker, J. P., van Gorkom, H. J., Brok, M., and Ouwehand, L. (1984) Optical characterization of photosystem II electron donors, *Biochim. Biophys. Acta* **764**, 301–309.
33. Jensen, D., and Barry, B. (2009) Proton-coupled electron transfer in Photosystem II: Proton inventory of a redox active tyrosine, *J. Am. Chem. Soc.* **131**, 10567–10573.
34. Jensen, D., Evans, A., and Barry, B. (2007) Proton-coupled electron transfer and tyrosine D of photosystem II, *J. Phys. Chem. B* **111**, 12599–11264.
35. Rappaport, F., Boussac, A., Force, D., Pelloquin, J., Bryndal, M., Sugiyama, M., Un, S., Britt, D., and Diner, B. (2009) Probing the coupling between proton and electron transfer in photosystem II core complexes containing a 3-fluorotyrosine, *J. Am. Chem. Soc.* **131**, 4425–4433.
36. Ferreira, K. N., Iverson, T. M., Maghlaoui, K., Barber, J., and Iwata, S. (2004) Architecture of the photosynthetic oxygen-evolving center, *Science* **303**, 1831–1838.
37. Guskov, A., Kem, J., Gabdulkhakov, A., Boser, M., Zouni, A., and Saenger, W. (2009) *Nat. Struct. Mol. Biol.* **19**, 334–342.
38. Moser, C., Page, C., Farid, R., and Dutton, P. (1995) Biological electron transfer, *J. Bioenerg. Biomembr.* **27**, 263–274.
39. Rhile, I. J., Markle, T. F., Nagao, H., DiPasquale, A. G., Lam, O. P., Lockwood, M. A., Rotter, K., and Mayer, J. (2006) Concerted proton-electron transfer in the oxidation of hydrogen-bonded phenols, *J. Am. Chem. Soc.* **128**, 6075–6088.
40. Lomoth, R., Magnuson, A., Sjödin, M., Huang, P., Styring, S., and Hammarström, L. (2006) Mimicking the electron donor side of photosystem II in artificial photosynthesis, *Photosynth. Res.* **87**, 25–40.
41. Irebo, T., Reece, S. Y., Sjödin, M., Nocera, D. G., and Hammarström, L. (2007) Proton-coupled electron transfer of tyrosine oxidation: buffer dependence and parallel mechanisms, *J. Am. Chem. Soc.* **129**, 15462–15464.
42. Costentin, C., Louault, C., Robert, M., and Savéant, J.-M. (2009) The electrochemical approach to concerted proton-electron transfers in the oxidation of phenols in water, *Proc. Nat. Acad. Sci. U.S.A.* **106**, 18143–18148.
43. Di Bilio, A. J., Crane, B. R., Wehbi, W. A., Kiser, C. N., Abu-Omar, M. M., Carlos, R. M., Ruchards, J. H., Winkler, J. R., and Gray, H. B. (2001) Properties of photogenerated tryptophan and tyrosyl radicals in structurally characterized proteins containing rhenium(II) tricarbonyl diimines, *J. Am. Chem. Soc.* **123**, 3181–3182.
44. Gasteiger, E., Gattiker, A., Hoogland, C., Ivanyi, I., Appel, R. D., and Bairoch, A. (2003) ExPASy: The proteomics server for in-depth protein knowledge and analysis, *Nucleic Acids Res.* **31**, 3784–3788.
45. Waters, M. L. (2004) Aromatic interactions in peptides: Impact on structure and function, *Biopolymers* **76**, 435–445.
46. Smith, C. K., and Regan, L. (1995) Guidelines for protein design: The energetics of β sheet side chain interactions, *Science* **270**, 980–982.
47. Ishimitsu, T., Hirose, S., and Sakurai, H. (1976) Acid dissociation of tyrosine and its related compounds, *Chem. Pharm. Bull. (Tokyo)* **24**, 3195–3198.
48. Ayala, I., Range, K., York, D., and Barry, B. A. (2002) Spectroscopic properties of tyrosyl radicals in dipeptides, *J. Am. Chem. Soc.* **124**, 5496–5505.
49. Vassiliev, I. R., Offenbacher, A. R., and Barry, B. A. (2005) Redox-active tyrosine residues in pentapeptides, *J. Phys. Chem. B* **109**, 23077–23085.
50. Barry, B. A., El-Deeb, M. K., Sandusky, P. O., and Babcock, G. T. (1990) Tyrosine radicals in PS II and related model compounds. Characterization by isotopic labeling and EPR spectroscopy, *J. Biol. Chem.* **265**, 20139–20143.
51. Johnson, C. W. (1988) Secondary structure of proteins through circular dichroism spectroscopy, *Annu. Rev. Biophys. Biophys. Chem.* **17**, 145–166.

52. Searle, M. (2001) Peptide models of protein β -sheets: Design, folding and insights in stabilizing weak interactions, *J. Chem. Soc., Perkin Trans. 2*, 1011–1020.
53. Ovchinnikova, T. V., Shenkarev, Z. O., Nadezhdin, K. D., Balandin, S. V., Zhmak, M. N., Kudelina, I. A., Finkina, E. I., Kokryakov, V. N., and Arseniev, A. A. (2007) Recombinant expression, synthesis, purification, and solution structure of arenicin, *Biochem. Biophys. Res. Commun.* 360, 156–162.
54. Maynard, A. J., Sharman, G. J., and Searle, M. (1998) Origin of β -hairpin stability in solution: Structural and thermodynamic analysis of the folding of a model peptide supports hydrophobic stabilization in water, *J. Am. Chem. Soc.* 120, 1996–2007.
55. Gallivan, J., and Dougherty, D. (1999) Cation- π interactions in structural biology, *Proc. Nat. Acad. Sci. U.S.A.* 96, 9459–9464.
56. Hilario, J., Kubelka, J., and Keiderling, T. A. (2003) Optical spectroscopic investigations of model β -sheet hairpins in aqueous solution, *J. Am. Chem. Soc.* 125, 7562–7574.
57. Moraes, L. G. M., Fazio, M. A., Vieira, R., F.F., Nakaie, C., R., Miranda, M. T. M., Schreier, S., Daffre, S., and Miranda, A. (2007) Conformational and functional studies of gomesin analogues by CD, EPR and fluorescence spectroscopies, *Biochim. Biophys. Acta* 1768, 52–58.
58. Moore, G., Pettigrew, G. (1990) *Cytochromes c. Evolutionary, Structural, and Physicochemical Aspects*, Springer–Verlag, Berlin.